THE JOURNAL OF PHYSICAL CHEMISTRY C
A JOURNAL OF THE AMERICAN CHEMICAL SOCIETY

pubs.acs.org/JPCC

Perspective

Tip-Enhanced Raman Imaging of Photocatalytic Processes at the Nanoscale

Stanislav Rizevsky and Dmitry Kurouski*

Cite This: https://doi.org/10.1021/acs.jpcc.2c03836

Read Online

ACCESS | Metrics & More | Article Recommendations

ABSTRACT: Over the past decade, tip-enhanced Raman spectroscopy (TERS), an emerging analytical technique that provides single-molecule sensitivity and subnanometer spatial resolution, was broadly utilized to investigate fundamental physics of plasmon-driven catalysis, as well as to examine photocatalytic properties on mono and bimetallic nanostructures. In TERS, coherent oscillations of conductive electrons, which are also known as localized surface plasmon resonances (LSPRs), are induced by light at the apex of metalized scanning probes. LSPRs (i) enhance Raman scattering from molecules located directly under the scanning probe, as well as (ii) decay producing hot carriers, highly energetic species that can catalyze a large spectrum of chemical reactions. Consequently, TERS allows for both in situ catalysis and visualization of chemical reactions in the probe-sample junction. This Perspective critically discusses mechanism of plasmon-driven catalysis and photocatalytic properties of noble metal nanomaterials. It also demonstrates the advantage of TERS in nanoscale imaging of photocatalytic reactions on bimetallic nanostructures, including gold−platinum and gold−palladium nanoplates. Finally, this Perspective provides an outlook for the future of TERS in photochemistry and material sciences.

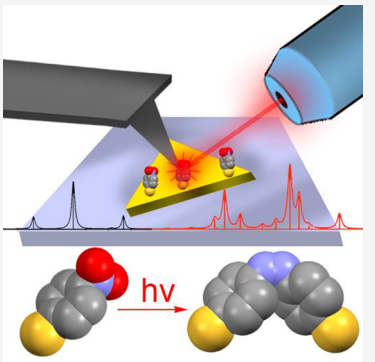

INTRODUCTION

If illuminated by light, noble metal nanostructures (NMNS) can generate collective oscillations of conductive electrons, which are also known as localized surface plasmon resonances (LSPRs).[1−6] The LSPR energies depend on the size and shape of nanostructures, as well as the material and local dielectric environment.[7,8] Therefore, a large number of synthetic approaches are available for fabrication of the nanostructures with desired optical properties.[7,9,10] LSPRs enable 100−1000-fold enhancement of the electric field in the vicinity of metallic nanostructures, which, in turn, results in up to 10^{12} enhancement of Raman scattering from molecules present on or near metal surfaces.[11−14] This physical phenomenon determines the extremely high sensitivity of surface-enhanced Raman scattering (SERS), the analytical approach used in various research fields to detect ultralow concentrations of molecular analytes.[2,15−18]

Using thermal evaporation or "wet synthesis", NMNS can be grown at the apex of commercially available scanning probes employed in atomic force microscopy (AFM).[19−22] Scanning probes with similar plasmonic properties can be also fabricated from gold (Au) or silver (Ag) wires by their electrochemical etching. These metal probes are traditionally used in scanning tunneling microscopy (STM).[23,24] Consequently, illumination of such metalized or metal scanning probes by light generates LSPRs at the tip apex, which, in turn, enhance Raman scattering from molecules located directly under the probe.[25,26] The probe can be positioned at the point of interest or rastered above the sample surface. In the former case, chemical information about that specific surface location can be obtained. The latter case allows for an acquisition of a chemical map of the sample with subnanometer spatial resolution.[27,28] During the past decade, this analytical approach, known as tip-enhanced Raman spectroscopy (TERS), has been broadly utilized for a large variety of applications including electrochemistry,[25,29−31] solid-state physics,[32−35] polymer science,[36−38] and biology.[39−42]

LSPRs decay by radiative and nonradiative processes.[43,44] The radiative decay is typical for large NMNS. In this case, the energy dissipates, producing heat. Upon nonradiative decay, LSPRs produce hot carriers.[44−46] These highly energetic species persist over a few tens of femtoseconds and further decay via electron−electron or electron−phonon scattering.[47,48] If molecular analytes are present in the close proximity to the metal surfaces, hot carriers can be injected into electronic states of a nearby molecule inducing a large spectrum of chemical reactions.[49,50] Hot electrons and holes have unequal rates of dissipation from the metal surface.[51,52] This asymmetry results in the accumulation of hot carriers with "slower" dissipation rates between the nanostructure and the surrounding medium. Thus, light induces a "steady-state charge" or the "electrostatic potential" that can catalyze chemical reactions.[51,52] The electrostatic potential at different surface sites of NMNS can be quantified by TERS.[53] This

Received: June 2, 2022
Revised: July 6, 2022

information can be used to explain distinctly different catalytic reactivity exhibited by these surface locations.

It is important to emphasize that plasmonic heating, which is taken place in TERS, has very little if any effect on the chemical transformation observed in the tip−sample junction.[54,55] Using finite density time domain (FDTD) simulations, the Large group calculated light-induced temperature changes in tip−sample junction.[55] It was found that only a very small (∼40 K) increase in temperature could be expected in the metallized scanning probe when it was illuminated with 20−500 μW of 671 nm light. These findings are in a good agreement with experimental results recently reported by Richard-Lacroix and Deckert.[56] Using 16-mercaptohexadodecanoic acid as a molecular reporter, the researchers measured its Stokes and anti-Stokes TERS spectra at different intensities of 532 nm light. It was found that, at 100 uW, the temperature in the tip−sample junction reaches only ∼80 °C.[56] Similar findings were reported by the Frontiera group.[54] Specifically, Keller and Frontiera observed only a small, on the order of tens of Kelvin, temperature increase in the junction between two nanostructures, even for extremely high photoexcitation values.[54] These pieces of experimental evidence demonstrate that plasmon-driven chemistry observed in both TERS and SERS is not thermally driven.

TERS UNRAVELS THE NANOSCALE PHOTOCATALYTIC PROPERTIES OF NMNS AND THE UNDERLYING PHYSICS OF PHOTOREDUCTION

In 2012, Van Schrojenstein Lantman and co-workers reported the first in situ observation of a photocatalytic dimerization of 4-nitrobenzenethiol (4-NBT) into to *p,p′*-dimercaptoazobisbenzene (DMAB) that took place in the tip−sample junction.[57] Specifically, the researchers observed instantaneous dimerization of 4-NBT when the Ag-coated probe was illuminated by 532 nm light, whereas a substantially lower rate of 4-NBT to DMAB conversion was found if the same scanning probe was exposed to 633 nm laser light, Figure 1.[57] These observations suggested that the rate of photochemical transformations are determined by the LSPRs of the scanning probe.

As was discussed above, TERS allows for precise positioning the scanning probe at different surface sites of NMNS, including edges, corners, adatoms, and vacancies allowing for the direct elucidation of rates and yields of photochemical reactions at these locations. Using Au-coated scanning probe and 633 nm excitation, Li and Kurouski examined the nanoscale photocatalytic properties of Au nanoparticles (AuNPs), as well as their microplate (AuMPs) analogues.[58] It has been found that edges and corners of these nano- and microplates exhibited much greater yield of DMAB formed from 4-NBT than central parts of AuNPs, Figure 2a−d.[58]

Li and Kurouski hypothesized that a superior reactivity of the edges and corners of the nano- and microstructures was because of a greater intensity of the rectified electric field at these surface sites.[58] To test this hypothesis, the Kurouski group utilized 4-mercaptobenzonitrile (4-MBN) as a molecular probe.[53] A nitrile vibration of 4-MBN is highly sensitive to the intensity of rectified electric field.[59,60] The shift of this vibration, which is also known as a Stark shift, arises from a perturbation to the electronic environment of a chemical bond. Thus, the Stark shift can be used to quantify the strength of

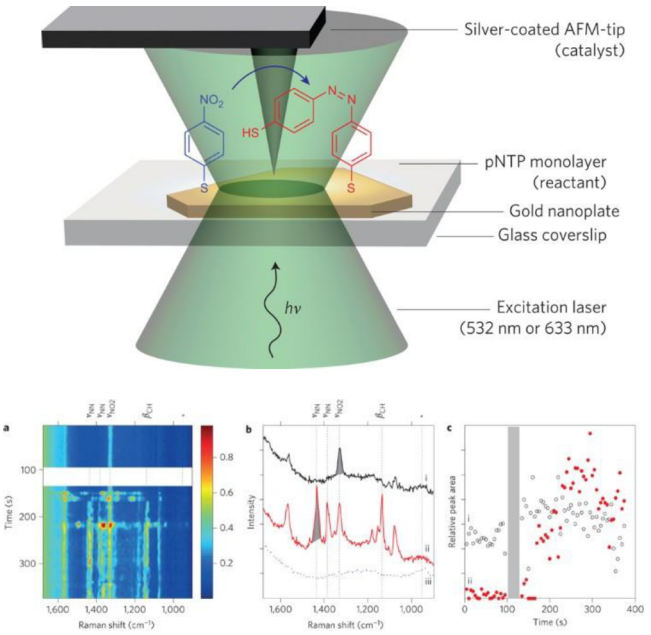

Figure 1. Top: Schematic illustration of the TERS experiment used to monitor the photocatalytic conversion of 4-NBT (blue) into DMAB (red) on AuNPs. Bottom: (a) Waterfall of TERS spectra collected with 633 nm excitation before (top) and after (below white band) illumination. (b) TERS spectra that correspond to 4-NBT (black) and DMAB (red). Spectrum (iii) is the reference spectrum taken after the time-dependent spectra. (c) Peak areas as a function of time for the 4-NTP band at 1335 cm^{-1} (i) and for the band at 1440 cm^{-1} (ii), belonging to DMAB. The period of green illumination between 100 and 130 s is indicated by the shaded band. Reprinted with permission from ref 57. Copyright 2012 Nature Springer.

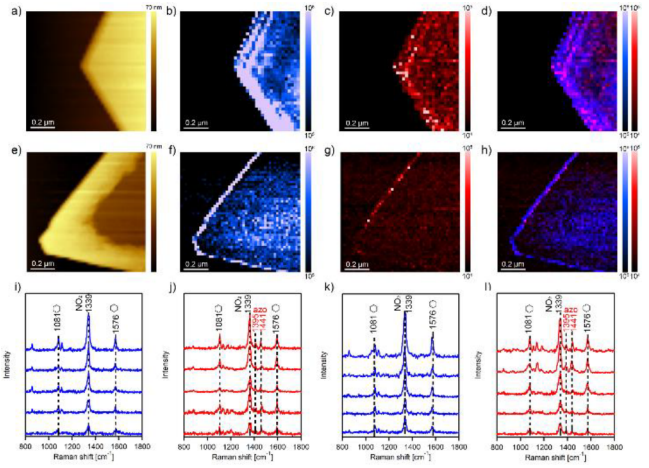

Figure 2. (a) AFM images of AuMPs and (e) WAuMPs. TERS images of (b, c, d) AuMPs and (f, g, h) WAuMPs (20 nm per pixel). The intensity of the 1339 cm^{-1} band (NO_2) of 4-NBT is shown in blue, intensities of 1397 and 1441 cm^{-1} (azo) of DMAB are shown in red. (i−l) Typical TERS spectra extracted from chemical maps on (b and f) showing the presence of 4-NBT (blue). Randomly picked TERS spectra from chemical maps shown in (c and g) demonstrate the presence of DMAB (red). Reprinted with permission from ref 67. Copyright 2021 Royal Society of Chemistry.

rectified electric field on the surface of AuNPs.[59,61] The reported results by Li and co-workers confirmed that edges and corners of AuNPs exhibited greater, on average, intensity of the rectified electric field than the central parts of the

https://doi.org/10.1021/acs.jpcc.2c03836
J. Phys. Chem. C XXXX, XXX, XXX−XXX

nanostructures.[53] Similar conclusions were independently made by the El-Khoury group that utilized TERS to examine photocatalytic properties of Ag nanoparticles (AgNPs) and Ag nanowires (AgNWs).[62,63] Researchers found that the rectified electric field was stronger at the edges and corners of NMNS in that at their flat terraces.[64,65] On the basis of these findings, one can conclude that catalytic reactivity of the NMNS is determined by the intensity of the rectified electric field on their surfaces.

It should be noted that, in solution, no direct correlation between the magnitude of the electric field and plasmon-driven reactivity of AuMPs was observed.[66] Specifically, Bhattarai and El-Koury noticed that plasmon-driven dimerization of 4-NBT did not take place at all surface sites of AuMPs with high local optical field enhancement. Furthermore, the researchers observed that, in solution, dimerization of 4-NBT is reversible and both trans and cis forms of DMAB could be formed.[66]

One can expect that the intensity of the rectified electric field is not the only factor that determines photocatalytic reactivity of NMNS. A growing body of evidence suggests that crystal facets and molecular orientation can play an important role in photocatalysis.[37,67] Wang and Kurouski recently reported that if heated to 400 °C for 30−120 min, AuMPs could build walls around the perimeter of a nanostructure.[68] The wall formation is caused by a migration of Au atoms from the edges of AuMPs toward the center of the nanostructure. The researchers demonstrated that wall-AuMPs (WAuMPs) exhibited higher reactivity in the electrocatalytic conversion of methanol compared to results with AuMPs at lower formal potential.[68] Using TERS, Li and co-workers investigated the extent to which thermal reshaping of the nanostructures changes their photocatalytic properties, Figure 2e−h.[67] It has been found that WAuMPs exhibited a nearly 16 times lower yield of DMAB compared to results with the intact nanostructures. The authors hypothesized that such a strong degradation of the catalytic reactivity of WAuMPs was because of a heat-induced deformation of their crystal structure, which took place upon thermal reshaping. Expanding upon this, Wang and Kurouski investigated the relationship between metal crystal facets and catalytic activity of AuMPs using 3D-TERS and transmission electron microscopy.[69] In 3D-TERS probes, the active zones present not only at the tip apex but also on the shaft of the scanning probe. This allows for probing the chemical reactivity of both sides and top surfaces of analyzed nanostructures. It has been found that Au (111) present on the top of AuMPs exhibited much higher rates of 4-NBT reduction by $NaBH_4$ than Au (100) and Au (110) facets located on the AuMPs sides, Figure 3.[69] These experimental results demonstrated that higher order facets exhibited greater reactivity in chemical reactions than lower order facets of AuMPs. It should be noted that, recently, Rossi and coauthors found that lower coordinated surface sites, such as corners and edges, as well as (100) facets demonstrated higher reactivity in plasmon-driven reactions than the higher coordinated surface sites such as (111) facets.[70] Thus, one can expect that more stable Au(111) facets exhibited greater reactivity in chemical, whereas Au(100) and Au(110) in in plasmon-driven reactions.

It should be noted that, in addition to the facets and the intensity of the rectified electric field, the density of molecular analytes on the metallic surfaces and their binding geometry play an important role in photocatalytic transformations. Specifically, the Zenobi group showed that lower packed areas of 4-NBT on AuNPs exhibited greater reactivity in DMAB

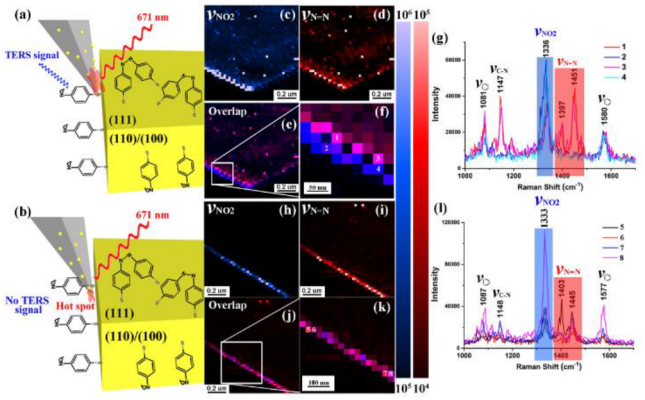

Figure 3. TERS imaging of the facet-dependent reduction of 4-NTP catalyzed by AuMPs. (a, b) Proposed schemes showing the hot-spot located at both the shaft and apex (a) and only at the apex (b) of the TERS probe. High resolution TERS images of the distribution of $-NO_2$ (c, h) and N═N groups (d, i) obtained with 3D TERS active and inactive probes, respectively. (e, j) Corresponding overlap of NO_2 and N═N images (c and d for e; h and i for j). (f, k) Zoomed-in TERS images of the white rectangle position in (e) and (j), respectively. (g, l) Typical TERS spectra extracted from the marked position in (f) and (k). Reprinted with permission from ref 69. Copyright 2018 American Chemical Society.

formation rather than thermodynamically stable ordered clusters of 4-NBT.[37] Thus, the density of molecular analytes on the plasmonic materials should be strongly considered in plasmon-driven photocatalysis. The Ren group demonstrated that on Au(111), rough Ag, and AgNPs and AuNPs, 4-aminothiophenol (4-ATP) is oriented at the angle relative to the metallic surfaces.[71] This molecular orientation determines instantaneous photocatalytic dimerization of 4-ATP into DMAB. However, strongly vertical orientation of this molecular analyte on Ag(111) prevents this plasmon-driven dimerization. The researchers attributed the stability of 4-ATP on Ag(111) to the π-stacking of aromatic moieties of these molecules.[71]

The question to ask is, how can this knowledge be used to measure kinetic and thermodynamic parameters of photocatalytic reactions? Recent findings reported by the Kurouski group[72] showed that TERS could be used to quantify the rates of photocatalytic reactions. Specifically, Li and Kurouski measured rates of 4-NBT to DMAB conversion on AuNPs at different intensities of the external electric field.[72] It has been found that with an increase in the electric field, the increase in the reaction rates was observed ($k_{30\mu w}$ = 0.126 s^{-1}, $k_{90\mu w}$ = 0.343 s^{-1}, and $k_{150\mu w}$ = 0.819 s^{-1}). The same experimental approach was utilized to determine rates of redox reaction between (4-mercaptophenyl)methanol (4-MPM) and 4-mercaptobenzoic acid (4-MBA).[73] These experimental findings revealed the direct relationship between an intensity of the external electric field and the rates of photocatalytic reactions on NMNS.

NANOSCALE IMAGING OF PHOTOCATALYSIS ON BIMETALLIC NANOSTRUCTURES (BMNS)

Localization of NMNS in a proximity to nanostructures fabricated from catalytic metals, such as palladium (Pd), ruthenium (Ru), or platinum (Pt), allows for transitioning of LSPRs generated on NMNS to these catalytic counterparts.[74] The catalytic nanostructures, in turn, are capable of performing

https://doi.org/10.1021/acs.jpcc.2c03836
J. Phys. Chem. C XXXX, XXX, XXX−XXX

a much broader spectrum of chemical reactions compared to the reactions observed on NMNS.[14,74] Noble and catalytic metals may also form an alloy or can be simply copresent in one nanostructure in a "sandwich-like" geometry.[74] A growing body of evidence suggests that the interplay between plasmonic and catalytic metals, as well as the nanoscale localization of these two metals, determines the yield of photocatalytic reactions.[32,33] Therefore, TERS imaging of BMNS can be used to tailor synthetic procedures that will allow for the fabrication of BMNS with desired photocatalytic properties.

In 2017, the Ren group utilized phenyl isocyanide (PIC) as a molecular reporter to investigated the nanoscale reactivity of submonolayer of Pd on Au surface.[75] It was found that TERS spectra collected at Pd edges exhibited a 60 cm^{-1} red shift of the C≡N vibration compared to the frequency of C≡N in the spectra collected from Pd atoms located in terraces, Figure 4a–c. These results indicated that a degree of back-donation from the d band of the metal to the antibonding π^* orbital of PIC at the step site is greater than at the terrace sites. These findings suggest that molecules located at Pd edges have higher reactivity than Pd atoms present in terraces. A similar approach was utilized by the Ren group to examine the electronic properties of a Pt nanoisland on Au surfaces.[76] The researchers observed a blue shift of the C≡N vibration of 4-chlorophenyl isocyanide, similar to the PIC molecular reporter, in TERS spectra collected from lower coordinated Pt sites in which a higher d-band center was expected, Figure 4d–g. These findings pointed to the drastic difference in the electronic structures between Pt and Pd, which, in turn, could be used to explain differences in molecule–metal interaction that are taken place in the case of these two catalytic metals.

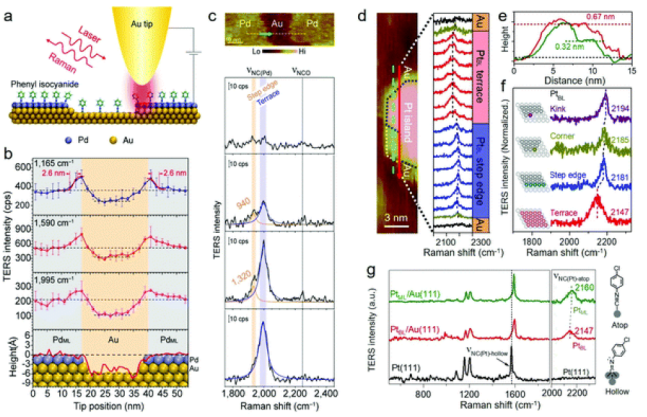

Figure 4. (a) Sketch of TERS experiments used to probe reactivity of Pd@Au(111) surfaces. (b) Intensity of TERS spectra collected from the Pd step edge with 3 nm spatial resolution. (c) STM image (top panel) and line-trace TERS spectra (bottom panel) along the green arrow in the STM image, showing a unique red-shifted νNC at the Pd step edge. (a–c) Reproduced with permission from ref 75. Copyright 2017 Nature Springer. (d) STM image of the Pt/Au(111) bimetallic surface (left panel) and line-trace TERS spectra (right panel) along the red arrow in the STM image. (e) Height profiles along the green and red lines in (d). (f) Site-specific νNC peaks at Pt sites. (g) Bimetallic effects on PtML/Au(111), PtBL/Au(111), and Pt(111). (d–g) Reproduced with permission from ref 76. Copyright 2018 John Wiley & Sons, Inc.

Expanding upon this, the Kurouski group used TERS to analyze the nanoscale photocatalytic properties of gold–platinum nanoplates (Au@PtNPs).[58] It was found that Au@PtNPs could oxidize 4-ATP directly to 4-NBT. At the same time, under the same experimental conditions only DMAB was found on their monometallic analogues, AuNPs.[58,69,77] It should be noted that edges and corners of Au@PtNPs demonstrated substantially greater photocatalytic reactivity than flat terraces. Independently, Li and co-workers utilized TERS to examine photocatalytic properties of gold–palladium microplates (Au@PdMPs).[72] It was found that these bimetallic microstructures were capable of reducing 4-NBT to both 4-ATP and DMAB. Furthermore, edges of Pd clusters demonstrated the greatest yield of 4-ATP, whereas valleys between the clusters produced primarily DMAB. It should be noted that the analogous photoreduction of 4-NBT on AuNPs yielded only DMAB. Using TERS, Li and co-workers also determined reaction rates of 4-NBT to DMAB reduction on the surface of Au@PdMPs at different intensities of the external electric field.[72] It has been found that an increase in the electric field caused a linear increase in the reaction rate of 4-NBT to DMAB conversion.[72] These results showed that light intensity could be used to control reaction rates not only on NMNS but also on BMNS.

Using TERS, the Kurouski group investigated photocatalytic properties of alloy-type and "sandwich-like" bimetallic nanostructures.[67] Specifically, the researchers examined the yield of plasmon-driven reduction of 4-NBT on "sandwich-like" Au@PdNPs and their alloy analogues, walled-Au@PdNPs (WAu@PdNPs). As was discussed above, the former bimetallic nanostructures have well-defined boundaries between Au and Pd atoms on their surface. The latter nanostructures were prepared by thermal heating of Au@PdNPs, which causes their reshaping and formation of walls around the perimeter of Au@PdNPs. Thermal heating also erases boundaries between Pd and Au, making both metals forge into an alloy. It was found that 4-NBT reduction on both Au@PdNPs and WAu@PdNPs yielded DMAB and 4-ATP, the reaction product that was not observed on the monometallic analogues of these nanostructures. Li and co-workers found that Au@PdNPs yield ∼65% of DMAB with only ∼6% of 4-ATP, whereas the yield of these products on WAu@PdNPs was ∼47% and ∼17%.[67] Thus, alloy-type bimetallic nanostructures yield a large amount of 4-ATP than their "sandwich-like" analogues. This study demonstrates how the interplay between catalytic (Pd) and plasmonic (Au) metals can alter the yield of plasmon-driven reactions on the bimetallic nanostructures.

The Ren and Zenobi groups recently reported an outstanding work on TERS imaging of catalytic hydrogenation of chloronitrobenzenethiol on Pd submonolayer present on Au (111) surface.[78] There researchers showed that catalytic hydrogenation occurred beyond the location of Pd sites and was observed as far as 20 nm from the bimetallic Pd/Au boundary. These findings suggest that the interplay between plasmonic and catalytic metals at the nanoscale is far more complex than it was previously expected.

An interesting chemistry on Au@PtNPs and Au@PdNPs was recently reported by Li and Kurouski.[73] The researchers found that Au@PtNPs could be used to oxidize 4-MPM to 4-MBA, whereas the reversed reduction of 4-MBA to 4-MPM was evident only for Au@PdNPs, Figure 5. Furthermore, none of these chemical transformations was possible without the catalytic metal present in the nanostructures. Specifically, on AuNPs, both 4-MBA and 4-MPM produced only thiophenol.

https://doi.org/10.1021/acs.jpcc.2c03836
J. Phys. Chem. C XXXX, XXX, XXX–XXX

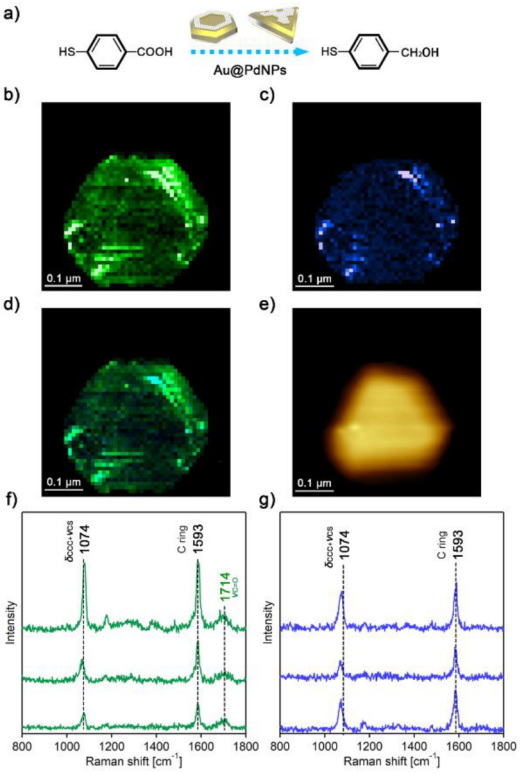

Figure 5. Plasmon-driven reduction of 4-MBA to 4-MPM on Au@PdNPs. (a) Schematic illustration of MBA reduction to MPM by Au@PdNPs. (b, c) TERS images of Au@PdNPs (10 nm per pixel). The intensity of 1570−1750 cm^{-1} containing the C ring vibration and the C═O vibration of 4-MBA is shown in green; the 1593 cm^{-1} band (C ring vibration) of MPM without showing the C═O vibration band (1714 cm^{-1}) is shown in blue. (d) Overlapping TERS image of 4-MPM and 4-MBA. (e) In situ AFM image of Au@PdNPs during TERS imaging. (f, g) Typical TERS spectra extracted from chemical maps on Au@PdNPs (a, b) showing presence of 4-MPM (blue) and 4-MBA (green). Reprinted with permission from ref 73. Copyright 2021 American Chemical Society.

These findings demonstrated that Pt determines unique oxidation, whereas Pd unique reduction properties of BMNS.

On the basis of the findings discussed above, one can conclude that photochemistry at the nanoscale depends on

- LSPRs of the scanning probe, which in turn depend on the metal used for the probe fabrication, and excitation wavelength (it should be noted that if LSPRs of analyzed NMNS and BMNS are within the excitation wavelength used in TERS, plasmonic coupling between the scanning probe and the nanostructures should be considered)
- the geometry and crystal facets of NMNS and BMNS
- the density and binding geometry of molecular analytes on the metal surface
- interplay between plasmonic and catalytic metals

FUTURE PERSPECTIVES: NOVEL CHEMISTRY AND NOVEL MATERIALS

The discussed above studies highlighted the potential of TERS in the nanoscale analysis of plasmon-induced chemical transformations. One can envision that these advantages of TERS will be utilized in the future to unravel kinetics, thermodynamics, as well as mechanisms of novel chemical reactions at gas−solid and liquid−solid interfaces. For instance, recently reported findings by the Kurouski group demonstrated that TERS could be used to probe molecular reactivity of aromatic halides in the Suzuki−Miyaura coupling reaction.[79] Specifically, the researchers were able to determine the reactivity of 4-bromo-, 4-chloro-, and 4-fluorothiophenols (4-BTP, 4-CTP, and 4-FTP) in the Suzuki−Miyaura coupling reaction with 4-mercaptophenylboronic acid (4-MPBA), Figure 6.

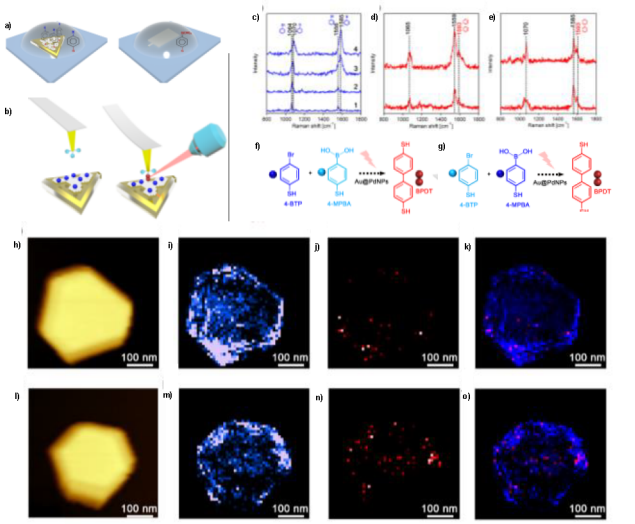

Figure 6. (a) Scheme of chemical modification of Au@PdNPs with 4-BTP and Au-coated scanning probes with 4-MPBA. (b) Plasmon-driven Suzuki−Miyaura coupling of 4-MPBA and 4-BTP on the surface of Au@PdNPs that yields biphenyl-4,4-dithiol (BPDT). (c) Representative TERS spectra of 4-BTP (1,2) and 4-MPBA (3,4) on the surface of Au@PdNPs. (d) SERS of 4-MPBA (5,6) and 4-BTP (7,8) on an Au-coated probe. (e) TERS spectra of BPDT on Au@PdNPs. (f) Schematic representation of the Suzuki−Miyaura coupling reaction between 4-BTP-modified Au@PdNPs and the 4-MPBA-modified Au-coated probe. (g) Schematic representation of the Suzuki−Miyaura coupling reaction between the 4-BTP-modified Au-coated probe and 4-MPBA-modified Au@PdNPs. (h) AFM and the corresponding TERS image of 4-BTP-modified Au@PdNPs (i) before the Suzuki−Miyaura coupling reaction and (j) after demonstrating the formation of BPDT (red pixels). (k) Overlay TERS image of 4-BTP (blue) and BPDT (red) signals on Au@PdNPs. (l) AFM and the corresponding. TERS image of 4-MPBA-modified Au@PdNPs (m) before the Suzuki−Miyaura coupling reaction and (n) after demonstrating the formation of BPDT (red pixels). (o) Overlay TERS image of 4-MPBA (blue) and BPDT (red) signals on Au@PdNPs. The scale bar in each image is 100 nm. Reprinted with permission from ref 79. Copyright 2021 Royal Society of Chemistry.

Using TERS, Wang and co-workers discovered a novel class of plasmon-driven chemical transformations that was caused by ionization of molecular analytes. Specifically, the researchers found that 4-NBT could be converted into 4-nitrobenzothiolate (4-NBT^-) on the surface of AuNPs.[77] This conclusion was made by an observation of the shift of 1335 cm^{-1} vibration of 4-NBT to 1305 cm^{-1} of 4-NBT^-.[77] Expanding upon these findings, the El-Khoury group reported experimental evidence of 4-NBT ionization on Ag nanoparticles.[35] Furthermore, the researchers found that if on AuNPs only ∼1.5% of all 4-NBT molecules are ionized, Ag yields 100% ionization of 4-NBT in the tip−sample junction. Thus, the molecular ionization yield is determined by the nature of the plasmonic metal. These findings, as well as a recently reported study by O'Callahan and

https://doi.org/10.1021/acs.jpcc.2c03836
J. Phys. Chem. C XXXX, XXX, XXX−XXX

El-Khoury,[80] demonstrate the importance of density functional theory (DFT) in elucidation of spectroscopic changes observed upon TERS imaging of molecular analytes on the surface of NMNS.

One may also envision that unique nanoscale imaging properties of TERS will be utilized to improve the understanding about the physics of 2D and 3D materials. For instance, the Gogotsi group utilized TERS to analyze single-layer and few-layer flakes of $Ti_3C_2T_x$ MXene deposited on a gold substrate.[33] The researchers found that TERS could be used to reveal the environmental stability of stoichiometric single-layer MXenes and showed that the intensity of TERS responses from the single- and few-layer flakes of $Ti_3C_2T_x$ could be used to track early stages of degradation, well before significant morphological changes appear. The Kurouski group reported that TERS could be used to probe the photochemistry on copper nanocubes and nanowires (CuNCs and CuNWs, respectively).[81] The researchers reported that both CuNCs and CuNWs were able to reduce 4-NBT to DMAB, as well as oxidize 4-MPM to 4-MBA. However, the reversed reduction of 4-MBA to 4-MPM was not evident on Cu nanomaterials because of strong interactions of the carboxylic group of 4-MBA with Cu, which prevents its reduction.

Ultrahigh vacuum (UHV) TERS offers (i) direct visualization of molecular analytes with angstrom spatial resolution and (ii) precise control of the molecular environment.[23,24,82,83] Using the advantage of UHV-TERS, the Hou and Jiang groups were able to probe weak molecule−substrate interactions and conformations of molecular analytes on the metal surfaces.[82,84−87] Furthermore, Xu and co-workers demonstrated that an electric field of the scanning probe can be used to trigger conformational changes in pentacene adsorbed on Ag(110).[86] Specifically, the researchers observed α to γ conformational changes in the central benzene ring of pentacene. These changes are characterized by ring expansion along the long molecular axis. Using TERS, the researchers demonstrated that α to γ conformational changes were caused by C−H bond breaking at the central benzene ring of pentacene followed by the skeleton deformation of this molecule. Recently, the Jiang group reported that a scanning probe could be used to trigger a dissociation of specific molecular site (C−Si bond) in individual 5,10,15,20-tetrakis-[(trimethylsilyl)ethynyl]porphyrin molecules adsorbed on a Cu(100) surface, Figure 7.[84] To enable such bond scissoring, the scanning probe had to be positioned precisely at the chemical bond atop the molecule. These findings confirmed the discussed above property of the scanning probes used in TERS to trigger photochemical transformation in the molecular analytes present on metallic surfaces.

■ PROBLEMS AND CHALLENGES FACED BY TERS

Although discovered more than 20 years ago,[88−90] TERS to a large extent remains a technique used only by around a dozen laboratories around the world. Primarily because of several problems that remain unsolved for decades.

Robust and Reliable Scanning Probes. Although numerous synthetic solutions were reported to date,[91] there are no reliable methods that could be used to fabricate reproducible and reliable scanning probes. Most of laboratories prepare their own scanning probes by simple thermal deposition of plasmonic metals[40,41,56,58,73,79,81,92,93] or electrochemical etching of Au or Ag wires.[23,24,82,83] Both of these methods do not provide desired reproducibility of scanning probes. Although the exact yield of such fabrication approaches was never reported, thermal deposition of Au in our laboratory yields ∼40% of tips suitable for TERS imaging.

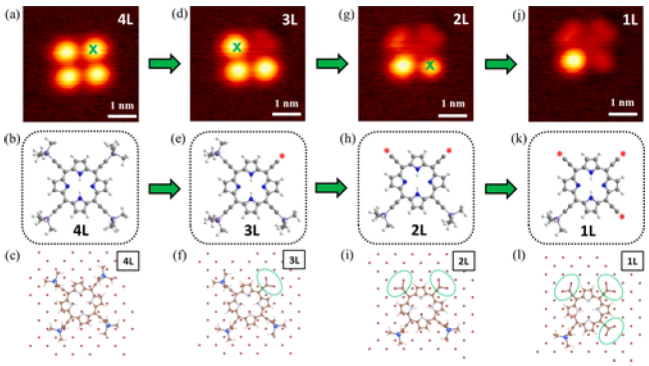

Figure 7. Consecutive C−Si bond dissociations in individual 5,10,15,20-tetrakis[(trimethylsilyl)ethynyl]porphyrin molecule. STM image, ball-and-stick model, and calculated adsorption geometry (top view) for 4L (a, b, c), 3L (d, e, f), 2L (g, h, i), and 1L (j, k, l), respectively. Reprinted with permission from ref 84. Copyright 2022 American Chemical Society.

Probe Contaminations. The most disappointing and hardly soluble problem of TERS is a spontaneous contamination of scanning probes. Any molecular analyte (even carbon nanotubes) can be easily transferred from a sample to the scanning probe upon TERS imaging. Although contaminated scanning probes can be cleaned and reused,[91] tip contamination enormously slows down TERS experiments. It should be noted that the evidence of the tip contamination can be easily found if the probe is withdrawn from the surface and then illuminated by light. The presence of the analyte fingerprint in such "tip-off" spectra indicates their contamination.

Lifetime of Scanning Probes. In most cases, the lifetime of scanning probes ranges from hours to days. Ag-coated scanning probes lose their enhancement fairly quickly because of the unavoidable oxidation of Ag by oxygen present in air. Obviously, UHV-TERS systems allow for the minimization of such oxidation.[23,24,82,83] Au-coated probes also lose their enhancement with time. One can expect that this is because of mechanical deformations of Au nanostructures present at the apex of the scanning probes. These deformations are caused by interactions between the scanning probe and the sample surface that take place upon TERS imaging in tapping and contact modes. There are several engineering approaches that can be used to protect metallized scanning probes from both abrupt contamination and oxidation.[91] For instance, the Sokolov group proposed to deposit several nanometers of aluminum (Al) on the top of silver or gold.[94] Al oxidation results in formation of a thin layer of Al_2O_3 that can protect the probe from a mechanic deformation. Although our laboratory could not reach the desired protection properties of Al_2O_3 either for Ag- or for Au-coated probes, the development of this and alternative tip-protection approaches can eventually solve the problem of tip contamination and improve the lifetime of the scanning probes.

There are also several challenges associated with TERS.

Interpretation of TERS Spectra. In TERS imaging of analytes with the simplest chemical structure, such as 4-NBT or 4-ATP, the appearance of random bands of unclear origin is commonly observed. Our group provided direct experimental

https://doi.org/10.1021/acs.jpcc.2c03836
J. Phys. Chem. C XXXX, XXX, XXX−XXX

and theoretical evidence that such peaks could be attributed to plasmon-driven reactions that are taken place in the tip−sample junction.[77] These findings suggest that TERS results should be treated far more carefully than was expected before. To a large extent, the evidence reported by our and other research groups[35,95−98] of hot-carrier reactivity of TERS limits the use of this highly powerful technique for the nanoscale analysis of complex, from the chemical perspective, samples.

Spatial Resolution. Although the angstrom-scale spatial resolution has been reported in UHV-TERS,[23,24,82,83] to a large extent this high resolution cannot be routinely archived in ambient TERS experiments.[35,95−98] These limitations root to relatively large values of thermal drifts of AFMs and the influence of environmental factors experienced in such AFM- and STM-TERS experiments. One can expect that development of most stable AFMs and minimization of the environmental factors by instrumental enclosures can solve this problem.

CONCLUSIONS

This Perspective summarized and critically reviewed the most recent findings on TERS-based imaging of photochemical transformation on NMNS and BMNS. These studies showed that TERS can be used to (i) trigger photochemical transformations in molecular analytes present on metallic surfaces and (ii) determine rates and yields of photochemical reactions at different surface sites, including edges and corners of the nanostructures. This information can be utilized to unravel reactivity of molecular analytes, as well as to determine kinetics and thermodynamics of novel photochemical reactions. Experimental results reported by Kurouski, and other research groups, also showed that TERS can be used to (iii) probe photocatalytic properties of NMNS and BMNS. One can expect that this knowledge will be utilized to tailor synthesis of novel nanostructures with desired photocatalytic properties.

Experimental results reviewed in this Perspective also helped to alter the perception of TERS in the scientific community. Although initially viewed solely as an imaging technique, TERS should be rather received as a tool that can be used to both catalyze and visualize chemical transformations. It should be noted that the preference in TERS-based catalysis vs imaging depends on a large number of factors that include crystal facets of metal sample, density of molecular analytes on the metal surface, and the interplay between plasmonic and catalytic metals. Finally, LSPRs of the scanning probe, which are determined by the metal used to fabricate the probe and excitation wavelength should be strongly considered for both tip-catalyzed photochemistry and tip-enhanced imaging at the nanoscale.

AUTHOR INFORMATION

Corresponding Author

Dmitry Kurouski − *Department of Biochemistry and Biophysics, Texas A&M University, College Station, Texas 77843, United States; Department of Biomedical Engineering, Texas A&M University, College Station, Texas 77843, United States; Institute for Advancing Health through Agriculture, College Station, Texas 77843, United States;* orcid.org/0000-0002-6040-4213; Phone: 979-458-3778; Email: dkurouski@tamu.edu

Author

Stanislav Rizevsky − *Department of Biochemistry and Biophysics, Texas A&M University, College Station, Texas 77843, United States; Department of Biotechnology, Binh Duong University, Thu Dau Mot 820000, Vietnam*

Complete contact information is available at: https://pubs.acs.org/10.1021/acs.jpcc.2c03836

Notes

The authors declare no competing financial interest.

Biographies

Stanislav Rizevsky earned his MS and Ph.D. in Biochemistry from Belarusian State University, Belarus. In 2014−2015, he was working as Head of Laboratory of Applied Biochemistry in the Biological Department at Belarusian State University. Since 2019, he has occupied a position of Vice Dean of the Biotechnology Department at Binh Duong University, Vietnam. In 2021, Dr. Rizevsky joined the Kurouski Lab in the Biochemistry and Biophysics Department of Texas A&M University as a Postdoc. Research interests are focused on amyloidogenic proteins, protein−lipid interactions, and secondary structure characterization using Infrared and Raman spectroscopy.

Dmitry Kurouski earned his MS in Biochemistry from Belarusian State University, Belarus, and his Ph.D. (Distinguished Dissertation) in Analytical Chemistry from SUNY Albany, NY, USA. After a Postdoc in the laboratory of Professor Richard P. Van Duyne at Northwestern University, Dr. Kurouski joined Boehringer-Ingelheim Pharmaceuticals, where he worked as Senior Research Scientist. In 2017, Dr Kurouski joined Biochemistry and Biophysics Department of Texas A&M University as Assistant Professor. His research interests are focused on nanoscale characterization of biological and photocatalytic systems using TERS and AFM-IR.

ACKNOWLEDGMENTS

We are grateful to AgriLife Research of Texas A&M for the provided financial support. We also acknowledge Governor's University Research Initiative (GURI) grant program of Texas A&M University, GURI Grant Agreement No. 12-2016, M1700437.

REFERENCES

(1) Kleinman, S. L.; Frontiera, R. R.; Henry, A. I.; Dieringer, J. A.; Van Duyne, R. P. Creating, Characterizing, and Controlling Chemistry with Sers Hot Spots. *Phys. Chem. Chem. Phys.* **2013**, *15*, 21−36.

(2) Brown, R. J.; Milton, M. J. T. Nanostructures and Nanostructured Substrates for Surface-Enhanced Raman Scattering (Sers). *J. Raman. Spectr.* **2008**, *39*, 1313−1326.

(3) Moskovits, M. Surface Roughness and the Enhanced Intensity of Raman Scattering by Molecules Adsorbed on Metals. *J. Chem. Phys.* **1978**, *69*, 4159−4161.

(4) Gersten, J.; Nitzan, A. Electromagnetic Theory of Enhanced Raman-Scattering by Molecules Adsorbed on Rough Surfaces. *J. Chem. Phys.* **1980**, *73*, 3023−3037.

(5) Kerker, M.; Wang, D. S.; Chew, H. Surface Enhanced Raman Scattering (Sers) by Molecules Adsorbed at Spherical Particles. *Appl. Opt.* **1980**, *19*, 3373−88.

(6) King, F. W.; Van Duyne, R. P.; Schatz, G. C. Theory of Raman Scattering by Molecules Adsorbed on Electrode Surfaces. *J. Chem. Phys.* **1978**, *69*, 4472−4481.

(7) Sharma, B.; Frontiera, R. R.; Henry, A. I.; Ringe, E.; Van Duyne, R. P. Sers: Materials, Applications, and the Future. *Mater. Today* **2012**, *15*, 16−25.

(8) Stiles, P. L.; Dieringer, J. A.; Shah, N. C.; Van Duyne, R. P. Surface-Enhanced Raman Spectroscopy. *Annu. Rev. Anal. Chem. (Palo Alto Calif)* **2008**, *1*, 601−26.
(9) Kleinman, S. L.; Frontiera, R. R.; Henry, A. I.; Dieringer, J. A.; Van Duyne, R. P. Creating, Characterizing, and Controlling Chemistry with Sers Hot Spots. *Phys. Chem. Chem. Phys.* **2013**, *15*, 21−36.
(10) Kurouski, D.; Lee, H.; Roschangar, F.; Senanayake, C. Surface-Enhanced Raman Spectroscopy: From Concept to Practical Application. *Scpectroscopy* **2017**, *32* (11), 36−44.
(11) Kelly, K. L.; Coronado, E.; Zhao, L. L.; Schatz, G. C. The Optical Properties of Metal Nanoparticles: The Influence of Size, Shape, and Dielectric Environment. *J. Phys. Chem. B* **2003**, *107*, 668−677.
(12) Wustholz, K. L.; Henry, A. I.; McMahon, J. M.; Freeman, R. G.; Valley, N.; Piotti, M. E.; Natan, M. J.; Schatz, G. C.; Van Duyne, R. P. Structure-Activity Relationships in Gold Nanoparticle Dimers and Trimers for Surface-Enhanced Raman Spectroscopy. *J. Am. Chem. Soc.* **2010**, *132*, 10903−10.
(13) Haes, A. J.; Haynes, C. L.; McFarland, A. D.; Schatz, G. C.; Van Duyne, R. P.; Zou, S. Plasmonic Materials for Surface-Enhanced Sensing and Spectroscopy. *MRS Bull.* **2005**, *30*, 368−375.
(14) Ringe, E.; McMahon, J. M.; Sohn, K.; Cobley, C.; Xia, Y.; Huang, J.; Schatz, G. C.; Marks, L. D.; Van Duyne, R. P. Unraveling the Effects of Size, Composition, and Substrate on the Localized Surface Plasmon Resonance Frequencies of Gold and Silver Nanocubes: A Systematic Single-Particle Approach. *J. Phys. Chem. C* **2010**, *114*, 12511−12516.
(15) Kurouski, D.; Large, N.; Chiang, N.; Greeneltch, N.; Carron, K. T.; Seideman, T.; Schatz, G. C.; Van Duyne, R. P. Unraveling near-Field and Far-Field Relationships for 3d Sers Substrates−a Combined Experimental and Theoretical Analysis. *Analyst* **2016**, *141*, 1779−1788.
(16) Henry, A. I.; Sharma, B.; Cardinal, M. F.; Kurouski, D.; Van Duyne, R. P. Surface-Enhanced Raman Spectroscopy Biosensing: In Vivo Diagnostics and Multimodal Imaging. *Anal. Chem.* **2016**, *88*, 6638−47.
(17) Kleinman, S. L.; Frontiera, R. R.; Henry, A. I.; Dieringer, J. A.; Van Duyne, R. P. Creating, Characterizing, and Controlling Chemistry with Sers Hot Spots. *Phys. Chem. Chem. Phys.* **2013**, *15*, 21−36.
(18) Sharma, B.; Frontiera, R. R.; Henry, A. I.; Ringe, E.; Van Duyne, R. P. Sers: Materials, Applications, and the Future. *Mater. Today* **2012**, *15*, 16−25.
(19) Kurouski, D. Advances of Tip-Enhanced Raman Spectroscopy (Ters) in Electrochemistry, Biochemistry, and Surface Science. *Vibrat. Specrosc.* **2017**, *91*, 3−15.
(20) Richard-Lacroix, M.; Zhang, Y.; Dong, Z.; Deckert, V. Mastering High Resolution Tip-Enhanced Raman Spectroscopy: Towards a Shift of Perception. *Chem. Soc. Rev.* **2017**, *46*, 3922−3944.
(21) Verma, P. Tip-Enhanced Raman Spectroscopy: Technique and Recent Advances. *Chem. Rev.* **2017**, *117*, 6447−6466.
(22) Sonntag, M. D.; Chulhai, D.; Seideman, T.; Jensen, L.; Van Duyne, R. P. The Origin of Relative Intensity Fluctuations in Single-Molecule Tip-Enhanced Raman Spectroscopy. *J. Am. Chem. Soc.* **2013**, *135*, 17187−92.
(23) Jiang, N.; Foley, E. T.; Klingsporn, J. M.; Sonntag, M. D.; Valley, N. A.; Dieringer, J. A.; Seideman, T.; Schatz, G. C.; Hersam, M. C.; Van Duyne, R. P. Observation of Multiple Vibrational Modes in Ultrahigh Vacuum Tip-Enhanced Raman Spectroscopy Combined with Molecular-Resolution Scanning Tunneling Microscopy. *Nano Lett.* **2012**, *12*, 5061−7.
(24) Klingsporn, J. M.; Jiang, N.; Pozzi, E. A.; Sonntag, M. D.; Chulhai, D.; Seideman, T.; Jensen, L.; Hersam, M. C.; Duyne, R. P. V. Intramolecular Insight into Adsorbate-Substrate Interactions Via Low-Temperature, Ultrahigh-Vacuum Tip-Enhanced Raman Spectroscopy. *J. Am. Chem. Soc.* **2014**, *136* (10), 3881−3887.
(25) Kurouski, D.; Mattei, M.; Van Duyne, R. P. Probing Redox Reactions at the Nanoscale with Electrochemical Tip-Enhanced Raman Spectroscopy. *Nano Lett.* **2015**, *15*, 7956−62.
(26) Kurouski, D.; Zaleski, S.; Casadio, F.; Van Duyne, R. P.; Shah, N. C. Tip-Enhanced Raman Spectroscopy (Ters) for in Situ Identification of Indigo and Iron Gall Ink on Paper. *J. Am. Chem. Soc.* **2014**, *136*, 8677−84.
(27) Zhang, R.; et al. Chemical Mapping of a Single Molecule by Plasmon-Enhanced Raman Scattering. *Nature* **2013**, *498*, 82−6.
(28) Lee, J.; Crampton, K. T.; Tallarida, N.; Apkarian, V. A. Visualizing Vibrational Normal Modes of a Single Molecule with Atomically Confined Light. *Nature* **2019**, *568*, 78−82.
(29) Zeng, Z. C.; Huang, S. C.; Wu, D. Y.; Meng, L. Y.; Li, M. H.; Huang, T. X.; Zhong, J. H.; Wang, X.; Yang, Z. L.; Ren, B. Electrochemical Tip-Enhanced Raman Spectroscopy. *J. Am. Chem. Soc.* **2015**, *137*, 11928−31.
(30) Martin Sabanes, N.; Ohto, T.; Andrienko, D.; Nagata, Y.; Domke, K. F. Electrochemical Ters Elucidates Potential-Induced Molecular Reorientation of Adenine/Au(111). *Angew. Chem., Int. Ed.* **2017**, *56*, 9796−9801.
(31) Pfisterer, J. H. K.; Baghernejad, M.; Giuzio, G.; Domke, K. F. Reactivity Mapping of Nanoscale Defect Chemistry under Electrochemical Reaction Conditions. *Nat. Commun.* **2019**, *10*, 5702.
(32) Yin, H.; et al. Nanometre-Scale Spectroscopic Visualization of Catalytic Sites During a Hydrogenation Reaction on a Pd/Au Bimetallic Catalyst. *Nat. Catal.* **2020**, *3*, 834−842.
(33) Sarycheva, A.; Shanmugasundaram, M.; Krayev, A.; Gogotsi, Y. Tip-Enhanced Raman Scattering Imaging of Single- to Few-Layer Ti3c2tx Mxene. *ACS Nano* **2022**, *16* (4), 6858−6865.
(34) Su, W.; Kumar, N.; Krayev, A.; Chaigneau, M. In Situ Topographical Chemical and Electrical Imaging of Carboxyl Graphene Oxide at the Nanoscale. *Nat. Commun.* **2018**, *9*, 2891.
(35) Wang, C. F.; O'Callahan, B. T.; Kurouski, D.; Krayev, A.; El-Khoury, P. Z. The Prevalence of Anions at Plasmonic Nanojunctions: A Closer Look at P-Nitrothiophenol. *J. Phys. Chem. Lett.* **2020**, *11*, 3809−3814.
(36) Opilik, L.; Payamyar, P.; Szczerbiński, J.; Schütz, A. P.; Servalli, M.; Hungerland, T.; Schlüter, A. D.; Zenobi, R. Minimally Invasive Characterization of Covalent Monolayer Sheets Using Tip-Enhanced Raman Spectroscopy. *ACS Nano* **2015**, *9*, 4252−4259.
(37) Cai, Z. F.; Merino, J. P.; Fang, W.; Kumar, N.; Richardson, J. O.; De Feyter, S.; Zenobi, R. Molecular-Level Insights on Reactive Arrangement in on-Surface Photocatalytic Coupling Reactions Using Tip-Enhanced Raman Spectroscopy. *J. Am. Chem. Soc.* **2022**, *144*, 538−546.
(38) Dai, W.; Shao, F.; Szczerbiński, J.; McCaffrey, R.; Zenobi, R.; Jin, Y.; Schlüter, A. D.; Zhang, W. Synthesis of a Two-Dimensional Covalent Organic Monolayer through Dynamic Imine Chemistry at the Air/Water. *Interface. Angew. Chem. Int. Ed.* **2016**, *128*, 221−225.
(39) Böhme, R.; Mkandawire, M.; Krause-Buchholz, U.; Rösch, P.; Rödel, G.; Popp, J.; Deckert, V. Characterizing Cytochrome C States − Ters Studies of Whole Mitochondria. *Chem. Commun.* **2011**, *47*, 11453−11455.
(40) Kurouski, D.; Deckert-Gaudig, T.; Deckert, V.; Lednev, I. K. Structure and Composition of Insulin Fibril Surfaces Probed by Ters. *J. Am. Chem. Soc.* **2012**, *134*, 13323−9.
(41) Kurouski, D.; Deckert-Gaudig, T.; Deckert, V.; Lednev, I. K. Surface Characterization of Insulin Protofilaments and Fibril Polymorphs Using Tip-Enhanced Raman Spectroscopy (Ters). *Biophys. J.* **2014**, *106*, 263−71.
(42) Lipiec, E.; Perez-Guaita, D.; Kaderli, J.; Wood, B. R.; Zenobi, R. Direct Nanospectroscopic Verification of the Amyloid Aggregation Pathway. *Angew. Chem., Int. Ed.* **2018**, *57*, 8519−8524.
(43) Liu, J. G.; Zhang, H.; Link, S.; Nordlander, P. Relaxation of Plasmon-Induced Hot Carriers. *ACS Photonics* **2018**, *5*, 2584−2595.
(44) Manjavacas, A.; Liu, J. G.; Kulkarni, V.; Nordlander, P. Plasmon-Induced Hot Carriers in Metallic Nanoparticles. *ACS Nano* **2014**, *8*, 7630−7638.

https://doi.org/10.1021/acs.jpcc.2c03836
J. Phys. Chem. C XXXX, XXX, XXX−XXX

(45) Khurgin, J. B. How to Deal with the Loss in Plasmonics and Metamaterials. *Nat. Nanotechnol.* **2015**, *10*, 2−6.
(46) Narang, P.; Sundararaman, R.; Atwater, H. A. Plasmonic Hot Carrier Dynamics in Solid-State and Chemical Systems for Energy Conversion. *Nanophotonics* **2016**, *5*, 96−111.
(47) Brown, A. M.; Sundararaman, R.; Narang, P.; Goddard, W. A., III; Atwater, H. A. Nonradiative Plasmon Decay and Hot Carrier Dynamics: Effects of Phonons, Surfaces, and Geometry. *ACS Nano* **2016**, *10*, 957−966.
(48) Hartland, G. V. Optical Studies of Dynamics in Noble Metal Nanostructures. *Chem. Rev.* **2011**, *111*, 3858−3887.
(49) Ma, J.; Wang, Z.; Wang, L.-W. Interplay between Plasmon and Single-Particle Excitations in a Metal Nanocluster. *Nat. Commun.* **2015**, *6*, 10107.
(50) Cortés, E.; Xie, W.; Cambiasso, J.; Jermyn, A. S.; Sundararaman, R.; Narang, P.; Schlücker, S.; Maier, S. A. Plasmonic Hot Electron Transport Drives Nano-Localized Chemistry. *Nat. Commun.* **2017**, *8*, 14880.
(51) Wilson, A. J.; Jain, P. K. Light-Induced Voltages in Catalysis by Plasmonic Nanostructures. *Acc. Chem. Res.* **2020**, *53*, 1773−1781.
(52) Yu, S.; Jain, P. K. The Chemical Potential of Plasmonic Excitations. *Angew. Chem., Int. Ed.* **2020**, *59*, 2085−2088.
(53) Li, Z.; Rigor, J.; Large, N.; El-Khoury, P.; Kurouski, D. Underlying Mechanisms of Hot Carrier-Driven Reactivity on Bimetallic Nanostructures. *J. Phys. Chem. C* **2021**, *125*, 2492−2501.
(54) Keller, E. L.; Frontiera, R. R. Ultrafast Nanoscale Raman Thermometry Proves Heating Is Not a Primary Mechanism for Plasmon-Driven Photocatalysis. *ACS Nano* **2018**, *12*, 5848−5855.
(55) Wang, R.; Li, J.; Rigor, J.; Large, N.; El-Khoury, P.; Yu, R. A.; Kurouski, D. Direct Experimental Evidence of Hot-Carrier-Driven Chemical Processes in Tip-Enhanced Raman Spectroscopy (Ters). *J. Phys. Chem. C* **2020**, *124* (3), 2238−2244.
(56) Richard-Lacroix, M.; Deckert, V. Direct Molecular-Level near-Field Plasmon and Temperature Assessment in a Single Plasmonic Hotspot. *Light Sci. Appl.* **2020**, *9*, 35.
(57) van Schrojenstein Lantman, E. M.; Deckert-Gaudig, T.; Mank, A. J.; Deckert, V.; Weckhuysen, B. M. Catalytic Processes Monitored at the Nanoscale with Tip-Enhanced Raman Spectroscopy. *Nat. Nanotechnol.* **2012**, *7*, 583−586.
(58) Li, Z.; Kurouski, D. Elucidation of Photo-Catalytic Properties of Goldplatinum Bimetallic Nanoplates Using Tip-Enhanced Raman Spectroscopy. *J. Phys. Chem. C* **2020**, *124* (52), 28500−28509.
(59) Marr, J. M.; Schultz, Z. D. Imaging Electric Fields in Sers and Ters Using the Vibrational Stark Effect. *J. Phys. Chem. Lett.* **2013**, *4*, 3268−3272.
(60) Kwasnieski, D. T.; Wang, H.; Schultz, Z. D. Alkyl-Nitrile Adlayers as Probes of Plasmonically Induced Electric Fields. *Chem. Sci.* **2015**, *6*, 4484−4494.
(61) Nelson, D. A.; Schultz, Z. D. Influence of Optically Rectified Electric Fields on the Plasmonic Photocatalysis of 4-Nitrothiophenol and 4-Aminothiophenol to 4,4-Dimercaptoazobenzene. *J. Phys. Chem. C* **2018**, *122*, 8581−8588.
(62) Bhattarai, A.; Crampton, K. T.; Joly, A. G.; Kovarik, L.; Hess, W. P.; El-Khoury, P. Z. Imaging the Optical Fields of Functionalized Silver Nanowires through Molecular Ters. *J. Phys. Chem. Lett.* **2018**, *9*, 7105−7109.
(63) Bhattarai, A.; Novikova, I. V.; El-Khoury, P. Z. Tip-Enhanced Raman Nanographs of Plasmonic Silver Nanoparticles. *J. Phys. Chem. C* **2019**, *123*, 27765−27769.
(64) Mayevsky, A. D.; Funston, A. M. Control of Electric Field Localization by Three-Dimensional Bowtie Nanoantennae. *J. Phys. Chem. C* **2018**, *122*, 18012−18020.
(65) Yang, H.; Owiti, E. O.; Jiang, X.; Li, S.; Liu, P.; Sun, X. Localized Surface Plasmon Resonance Dependence on Misaligned Truncated Ag Nanoprism Dimer. *Nanoscale Res. Lett.* **2017**, *12*, 430.
(66) Bhattarai, A.; El-Khoury, P. Z. Nanoscale Chemical Reaction Imaging at the Solid-Liquid Interface Via Ters. *J. Phys. Chem. Lett.* **2019**, *10*, 2817−2822.
(67) Li, Z.; El-Khoury, P.; Kurouski, D. Tip-Enhanced Raman Imaging of Photocatalytic Reactions on Thermally-Reshaped Gold and Gold-Palladium Microplates. *Chem. Commun.* **2021**, *57*, 891−894.
(68) Wang, R.; Kurouski, D. Thermal Reshaping of Gold Microplates: Three Possible Routes and Their Transformation Mechanisms. *ACS Appl. Mater. Interfaces* **2019**, *11*, 41813−41820.
(69) Wang, R.; Kurouski, D. Elucidation of Tip-Broadening Effect in Tip-Enhanced Raman Spectroscopy (Ters): A Cause of Artifacts or Potential for 3d Ters. *J. Phys. Chem. C* **2018**, *122*, 24334−24340.
(70) Rossi, T. P.; Erhart, P.; Kuisma, M. Hot-Carrier Generation in Plasmonic Nanoparticles: The Importance of Atomic Structure. *ACS Nano* **2020**, *14*, 9963−9971.
(71) Sun, J.-J.; Su, H.-S.; Yue, H.-L.; Huang, S.-C.; Huang, T.-X.; Hu, S.; Sartin, M. M.; Cheng, J.; Ren, B. Role of Adsorption Orientation in Surface Plasmon-Driven Coupling Reactions Studied by Tip-Enhanced Raman Spectroscopy. *J. Phys. Chem. Lett.* **2019**, *10*, 2306−2312.
(72) Li, Z.; Wang, R.; Kurouski, D. Nanoscale Photocatalytic Activity of Gold and Gold-Palladium Nanostructures Revealed by Tip-Enhanced Raman Spectroscopy. *J. Phys. Chem. Lett.* **2020**, *11*, 5531−5537.
(73) Li, Z.; Kurouski, D. Probing the Redox Selectivity on Au@Pd and Au@Pt Bimetallic Nanoplates by Tip-Enhanced Raman Spectroscopy. *Acs Photonics* **2021**, *8*, 2112−2119.
(74) Sytwu, K.; Vadai, M.; Dionne, J. A. Bimetallic Nanostructures: Combining Plasmonic and Catalytic Metals for Photocatalysis. *Adv. Phys. X* **2019**, *4* (1), 1619480.
(75) Zhong, J. H.; Jin, X.; Meng, L.; Wang, X.; Su, H. S.; Yang, Z. L.; Williams, C. T.; Ren, B. Probing the Electronic and Catalytic Properties of a Bimetallic Surface with 3 Nm Resolution. *Nat. Nanotechnol.* **2017**, *12*, 132−136.
(76) Su, H. S.; Zhang, X. G.; Sun, J. J.; Jin, X.; Wu, D. Y.; Lian, X. B.; Zhong, J. H.; Ren, B. Real-Space Observation of Atomic Site-Specific Electronic Properties of a Pt Nanoisland/Au(111) Bimetallic Surface by Tip-Enhanced Raman Spectroscopy. *Angew. Chem., Int. Ed. Engl.* **2018**, *57*, 13177−13181.
(77) Wang, R.; Li, J.; Rigor, J.; Large, N.; El-Khoury, P.; Yu, R. A.; Kurouski, D. Direct Experimental Evidence of Hot-Carrier-Driven Chemical Processes in Tip-Enhanced Raman Spectroscopy (Ters). *J. Phys. Chem. C* **2020**, *124* (3), 2238−2244.
(78) Yin, H.; et al. Nanometre-Scale Spectroscopic Visualization of Catalytic Sites During a Hydrogenation Reaction on a Pd/Au Bimetallic Catalyst. *Nat. Catal.* **2020**, *3*, 834−842.
(79) Li, Z.; Kurouski, D. Probing the Plasmon-Driven Suzuki-Miyaura Coupling Reactions with Cargo-Ters Towards Tailored Catalysis. *Nanoscale* **2021**, *13*, 11793−11799.
(80) O'Callahan, B. T.; El-Khoury, P. Z. A Closer Look at Tip-Enhanced Raman Chemical Reaction Nanoimages. *J. Phys. Chem. Lett.* **2022**, *13*, 3886−3889.
(81) Li, Z.; Kurouski, D. Tip-Enhanced Raman Analysis of Plasmonic and Photocatalytic Properties of Copper Nanomaterials. *J. Phys. Chem. Lett.* **2021**, *12*, 8335−8340.
(82) Mahapatra, S.; Ning, Y.; Schultz, J. F.; Li, L.; Zhang, J. L.; Jiang, N. Angstrom Scale Chemical Analysis of Metal Supported Trans- and Cis-Regioisomers by Ultrahigh Vacuum Tip-Enhanced Raman Mapping. *Nano Lett.* **2019**, *19*, 3267−3272.
(83) Chiang, N.; et al. Conformational Contrast of Surface-Mediated Molecular Switches Yields Angstrom-Scale Spatial Resolution in Ultrahigh Vacuum Tip-Enhanced Raman Spectroscopy. *Nano Lett.* **2016**, *16*, 7774−7778.
(84) Mahapatra, S.; Schultz, J. F.; Li, L.; Zhang, X.; Jiang, N. Controlling Localized Plasmons Via an Atomistic Approach: Attainment of Site-Selective Activation inside a Single Molecule. *J. Am. Chem. Soc.* **2022**, *144*, 2051−2055.
(85) Mahapatra, S.; Schultz, J. F.; Ning, Y.; Zhang, J. L.; Jiang, N. Probing Surface Mediated Configurations of Nonplanar Regioisomeric Adsorbates Using Ultrahigh Vacuum Tip-Enhanced Raman Spectroscopy. *Nanoscale* **2019**, *11*, 19877−19883.

https://doi.org/10.1021/acs.jpcc.2c03836
J. Phys. Chem. C XXXX, XXX, XXX−XXX

(86) Xu, J.; et al. Determining Structural and Chemical Heterogeneities of Surface Species at the Single-Bond Limit. *Science* **2021**, *371*, 818−822.
(87) Zhang, Y.; Yang, B.; Ghafoor, A.; Zhang, Y.; Zhang, Y. F.; Wang, R. P.; Yang, J. L.; Luo, Y.; Dong, Z. C.; Hou, J. G. Visually Constructing the Chemical Structure of a Single Molecule by Scanning Raman Picoscopy. *Natl. Sci. Rev.* **2019**, *6*, 1169−1175.
(88) Anderson, M. S. Locally Enchanced Raman Spectroscopy with an Atomic Force Microscope. *Appl. Phys. Lett.* **2000**, *76*, 3130−3132.
(89) Stöckle, R. M.; Suh, Y. D.; Deckert, V.; Zenobi, R. Nanoscale Chemical Analysis by Tip-Enhanced Raman Spectroscopy. *Chem. Phys. Lett.* **2000**, *318*, 131−136.
(90) Hayazawa, N.; Inouye, Y.; Sekkat, Z.; Kawata, S. Metallized Tip Amplification of near-Field Raman Scattering. *Opt. Commun.* **2000**, *183*, 333−336.
(91) Huang, T. X.; Huang, S. C.; Li, M. H.; Zeng, Z. C.; Wang, X.; Ren, B. Tip-Enhanced Raman Spectroscopy: Tip-Related Issues. *Anal. Bioanal. Chem.* **2015**, *407*, 8177−95.
(92) Li, Z.; Kurouski, D. Plasmon-Driven Chemistry on Mono- and Bimetallic Nanostructures. *Acc. Chem. Res.* **2021**, *54*, 2477−2487.
(93) Li, Z.; Kurouski, D. Nanoscale Structural Characterization of Plasmon-Driven Reactions. *Nanophotonics* **2021**, *10*, 1657−1673.
(94) Agapov, R. L.; Sokolov, A. P.; Foster, M. D. Protecting Ters Probes from Degradation: Extending Mechanical and Chemical Stability. *J. Raman Spectrosc.* **2013**, *44*, 710−716.
(95) Singh, P.; Deckert-Gaudig, T.; Zhang, Z.; Deckert, V. Plasmon Induced Deprotonation of 2-Mercaptopyridine. *Analyst* **2020**, *145*, 2106−2110.
(96) Wang, C. F.; O'Callahan, B. T.; Kurouski, D.; Krayev, A.; Schultz, Z. D.; El-Khoury, P. Z. Suppressing Molecular Charging, Nanochemistry, and Optical Rectification in the Tip-Enhanced Raman Geometry. *J. Phys. Chem. Lett.* **2020**, *11*, 5890−5895.
(97) Szczerbinski, J.; Gyr, L.; Kaeslin, J.; Zenobi, R. Plasmon-Driven Photocatalysis Leads to Products Known from E-Beam and X-Ray-Induced Surface Chemistry. *Nano Lett.* **2018**, *18*, 6740−6749.
(98) Szczerbinski, J.; Metternich, J. B.; Goubert, G.; Zenobi, R. How Peptides Dissociate in Plasmonic Hot Spots. *Small* **2020**, *16*, e1905197.

https://doi.org/10.1021/acs.jpcc.2c03836
J. Phys. Chem. C XXXX, XXX, XXX−XXX